ELSEVIER

Contents lists available at ScienceDirect

Earth and Planetary Science Letters

www.elsevier.com/locate/epsl



Depletion ages and factors of MORB mantle sources

Youxue Zhang (张有学)*, Ting Gan (甘 婷)

Department of Earth & Environmental Sciences, the University of Michigan, Ann Arbor, MI 48109, USA



ARTICLE INFO

Article history:
Received 20 June 2019
Received in revised form 17 October 2019
Accepted 24 October 2019
Available online 13 November 2019
Editor: R. Dasgupta

Keywords:
mantle geochemistry
mantle evolution
depleted mantle composition
model age of sub-ridge mantle
Sr-Nd isotopes
mantle partial melting

ABSTRACT

Sr-Nd-Hf-Pb isotopes show that the depleted MORB mantle (DMM) is not homogeneous. The heterogeneity is attributed to different ages of depletion and/or various degrees of depletion for a given domain of DMM, as well as multiple depletion events, metasomatism, and mixing between DMM and other mantle components. A mid-ocean ridge basalt, in principle, should contain information about the depletion history of its mantle sources. Here we develop a model to extract the model depletion age and the composition of a MORB mantle source prior to MORB production using Sr-Nd isotopes or Sr-Hf isotopes in a MORB. The complexities of multiple depletion events, mixing, metasomatism, and enrichment are not addressed in this contribution. The model is based on two assumptions: (i) Isotope evolution in a MORB mantle follows a two-stage evolution model, the first stage in the primitive mantle from the beginning of the solar system to the time of mantle depletion at age T_d , and the second stage in the depleted mantle from age T_d to the present day. That is, there is only one single depletion event. The depletion age and degree of depletion of a given mantle source are to be determined. (ii) The trace element composition of a depleted mantle source corresponding to the given MORB can be related to a reference DMM by a log-linear relation with the compatibility index CoI (Zhang, 2014). Applying the two assumptions to the available and large MORB database (Gale et al., 2013), we calculate the global distribution of sub-ridge mantle age and composition. The results show: (i) Mean or reference MORB mantle composition of Salters and Stracke (2004) is close to the average depleted MORB mantle composition, whereas that of Workman and Hart (2005) is significantly more depleted than the average depleted MORB mantle. (ii) Model ages for sub-ridge mantle depletion are mostly between 0.8 to 3.0 Ga. (iii) There are large-scale patterns in depletion ages for sub-ridge mantle regions. For example, beneath Mid-Atlantic Ridge, mantle depletion ages are young (0.8 to 2.1 Ga) north of 30°N, older (1.6 to 4.5 Ga) between 25°N to 35°S), and mixed (0.6-4.4 Ga) south of 35°S. The Pacific sub-ridge mantle has a narrow range of model depletion ages of 1.6 to 3.0 Ga, with a mean of 2.3 Ga. Indian sub-ridge mantle has a younger mean depletion age of 1.7 Ga. These large-scale patterns reveal history of mantle depletion, mantle convection, and possible mixing between older and younger depleted mantles.

© 2019 Elsevier B.V. All rights reserved.

1. Introduction

Earth's mantle is heterogeneous, with various degrees of depletion and enrichment (Gast, 1968; Zindler and Hart, 1986; Hofmann, 2014). The depletion is generally thought to be due to prior mantle partial melting (Jacobsen and Wasserburg, 1979; Zindler and Hart, 1986; Hofmann, 2014), whereas the enrichment is often attributed to mixing with a variety of rock types subducted to the mantle and/or metasomatism by low-degree melts and fluids (Zindler and Hart, 1986; Workman et al., 2004; Jackson and Dasgupta, 2008; Hofmann, 2014). The depleted MORB mantle (DMM), the source of MORB, is itself isotopically heterogeneous (Zindler

and Hart, 1986; Hofmann, 2014), presumably due to variable degrees of partial melting and/or different ages of depletion prior to the recent MORB production. Thousands of MORB samples have been studied in terms of major and minor oxides, trace elements, and isotopes. However, no systematic examination of the mantle depletion history has been made.

In this report, we present a two-stage mantle evolution model for any piece of depleted mantle that generates a MORB, by assuming that the depletion of various incompatible elements is related to the compatibility index (CoI; Zhang, 2014). Using the model, both the depletion age of the mantle source and the incompatible trace element concentrations in the mantle source can be inferred from $^{87}\mathrm{Sr}/^{86}\mathrm{Sr}$ and $^{143}\mathrm{Nd}/^{144}\mathrm{Nd}$ isotope ratios in any given depleted basalt. The model age of mantle source depletion for a given basalt may also be referred to as residence age in the depleted mantle, and is conceptually similar to the residence age calculated

^{*} Corresponding author.

E-mail address: youxue@umich.edu (Y. Zhang).

from isotope ratios in crustal rocks (Goldstein et al., 1984; Moller et al., 1998) and peridotites (Shirey and Walker, 1998; Mallick et al., 2014). The model is applied to all available MORB data and the results are plotted on a global map to display the global pattern of mantle depletion ages.

2. Data

Sr-Nd isotope data for MORB are from a large dataset in the synthesis paper by Gale et al. (2013), plus new MORB data in recent literature (Beltenev et al., 2014; Skolotnev, 2014; Shinjo et al., 2015; Cousens et al., 2017; Kim et al., 2017; Yang et al., 2017; Zhang et al., 2018). Data for back-arc basins are not used. Hf isotope data are fewer and are discussed in the next section. Pb isotope data are not used as discussed in the next section. Because our model can only be applied to depleted mantle domains, only isotope ratios with depleted mantle signatures, i.e., $^{87} {\rm Sr}/^{86} {\rm Sr} < 0.70452$ and $^{143} {\rm Nd}/^{144} {\rm Nd} > 0.51263$, are used. Among a total of 895 data points that satisfy these criteria, a small number (26) of them are deemed to be outliers (see later discussion) and not used. All the used data are listed in Supplementary Table S1.

3. Model

3.1. Model basics

Our model estimates the depletion age and composition of the mantle source using isotope ratios in a MORB. The model assumes a two-stage mantle evolution, with the first stage in the primitive mantle (PM), and the second stage in a depleted mantle. In the context of this model, given the primitive mantle composition, an isotopic ratio (e.g., 143Nd/144Nd) in a depleted MORB depends on only two parameters: the parent/daughter ratio in the second-stage mantle (i.e., the depleted mantle) and the age of the depletion. When two isotopic ratios are used (e.g., 143 Nd/144 Nd and $^{87}\rm{Sr}/^{86}\rm{Sr}$), one unknown is the age of mantle depletion, and the other two unknowns ($^{147}\rm{Sm}/^{144}\rm{Nd}$ and $^{87}\rm{Rb}/^{86}\rm{Sr}$) may be related to the compatibility index (CoI) defined by Zhang (2014), meaning that two unknowns (147 Sm/144 Nd ratio and 87 Rb/86 Sr ratio in the given depleted mantle) are reduced to one unknown, from which the whole incompatible trace element pattern can be inferred. Therefore, from two isotopic ratios, ¹⁴³Nd/¹⁴⁴Nd and 87 Sr/ 86 Sr, both the mantle depletion age (T_d) and the trace element pattern in the depleted mantle may be solved.

For a zero-age MORB, the isotope evolution equations in a two-stage model are:

$$\begin{pmatrix}
\frac{87}{86} \frac{Sr}{Sr} \\
MORB
\end{pmatrix}_{MORB} = \begin{pmatrix}
\frac{87}{86} \frac{Sr}{Sr} \\
T_0
\end{pmatrix}_{T_0} + \begin{pmatrix}
\frac{87}{86} \frac{Rb}{86} \\
\frac{86}{Sr}
\end{pmatrix}_{PM} (e^{\lambda_{87}T_0} - e^{\lambda_{87}T_d})$$

$$+ \begin{pmatrix}
\frac{87}{86} \frac{Rb}{86} \\
\frac{86}{Sr}
\end{pmatrix}_{DM} (e^{\lambda_{87}T_d} - 1), \tag{1}$$

$$\begin{pmatrix}
\frac{143}{144} \frac{Nd}{Nd} \\
\frac{144}{Nd}
\end{pmatrix}_{MORB} = \begin{pmatrix}
\frac{143}{144} \frac{Nd}{Nd} \\
\frac{144}{Nd}
\end{pmatrix}_{T_0} + \begin{pmatrix}
\frac{147}{144} \frac{Sm}{Nd} \\
\frac{144}{Nd}
\end{pmatrix}_{PM} (e^{\lambda_{147}T_0} - e^{\lambda_{147}T_d})$$

$$+ \begin{pmatrix}
\frac{147}{144} \frac{Sm}{Nd} \\
\frac{144}{Nd}
\end{pmatrix}_{DM} (e^{\lambda_{147}T_d} - 1), \tag{2}$$

where T_0 is the age of the solar system (4.5673 Ga, Connelly et al., 2012), $T_{\rm d}$ is the depletion age of the specific mantle source, subscript PM is the primitive mantle, subscript DM is any specific depleted mantle source for a given basalt (not the reference depleted mantle of either Salters and Stracke, 2004 or Workman and Hart, 2005), λ_{87} (= 0.013972 By $^{-1}$, Villa et al., 2015) and λ_{147} (= 0.006539 By $^{-1}$, Bouvier et al., 2008) are decay constants of 87 Rb and 147 Sm, $(^{87}$ Sr) 86 Sr) 70 0 = 0.69877 (Gray et al., 1973)

is the initial 87 Sr/ 86 Sr ratio at the beginning of the solar system at $T_0=4.5673$ Ga, $(^{87}$ Rb/ 86 Sr) $_{PM}=0.0852$ (discussed later), and $(^{147}$ Sm/ 144 Nd) $_{PM}=0.1960$ (Jacobsen and Wasserburg, 1984; Bouvier et al., 2008). The ratio $(^{143}$ Nd/ 144 Nd) $_{T_0}$ is calculated from the present day 143 Nd/ 144 Nd =0.512630 (Bouvier et al., 2008) and $(^{147}$ Sm/ 144 Nd) $_{PM}=0.1960$ to be 0.506688. Hence, there are three unknowns in the above two equations: $T_{\rm d}$, $(^{87}$ Rb/ 86 Sr) $_{\rm DM}$, and $(^{147}$ Sm/ 144 Nd) $_{\rm DM}$. Note that in the context of our model, $(^{87}$ Rb/ 86 Sr) $_{\rm DM}$ and $(^{147}$ Sm/ 144 Nd) $_{\rm DM}$ ratios are specific to the given depleted mantle region, and cannot be replaced by 87 Rb/ 86 Sr and 147 Sm/ 144 Nd in a reference depleted mantle (Salters and Stracke, 2004 or Workman and Hart, 2005).

To reduce the number of unknowns, we make the key assumption that the elemental composition of a given depleted mantle is related to the compatibility index CoI defined by Zhang (2014). For a given element i, the CoI value is defined as (Zhang, 2014):

$$CoI_i = ln(C_{i,RDM}/C_{i,PM}), \tag{3}$$

where RDM is a reference depleted mantle. There are two reference (average) depleted mantle compositions in literature, one by Salters and Stracke (2004), referred hereafter as RDM1, and the other by Workman and Hart (2005), referred hereafter as RDM2. These are independent efforts by different groups of scholars and they provide independent checks. The compositions of the two RDMs are well correlated (see discussion later).

The depletion factor z characterizes how the composition of a specific depleted mantle is related to the composition of the primitive mantle (PM) as follows

$$C_{i,\text{DM}} = C_{i,\text{PM}} \times \exp(zX_i),\tag{4}$$

where C is concentration, i means an element, X_i denotes CoI value for element i (CoI $_i$), and z is the depletion factor for the specific DM. If z = 0, there is no depletion; if z = 1, the given depleted mantle is the same as the RDM. We can hence derive:

$$(^{87}\text{Rb}/^{86}\text{Sr})_{\text{DM}} = (^{87}\text{Rb}/^{86}\text{Sr})_{\text{PM}} \times \exp[z(X_{\text{Rb}} - X_{\text{Sr}})],$$

$$(^{147}\text{Sm}/^{144}\text{Nd})_{\text{DM}} = (^{147}\text{Sm}/^{144}\text{Nd})_{\text{PM}} \times \exp[z(X_{\text{Sm}} - X_{\text{Nd}})],$$

$$(6)$$

where $(X_{\rm Rb}-X_{\rm Sr})=-1.1765$ and $(X_{\rm Sm}-X_{\rm Nd})=0.1717$ using RDM1 (see discussion below for adjustment of these values). Hence, there is only one unknown (z) for obtaining both $(^{87}{\rm Rb}/^{86}{\rm Sr})_{\rm DM}$ and $(^{147}{\rm Sm}/^{144}{\rm Nd})_{\rm DM}$. Therefore, Eqs. (1) and (2) contain only two unknowns $(T_{\rm d}$ and z), which can be solved from the two equations. Once z is solved, the concentration in the specific DM that generated the given MORB for any trace element with known CoI value can be calculated using Eq. (4). Combining the equations, we obtain:

$$z = \frac{1}{(X_{Rb} - X_{Sr})} \times \ln \frac{(\frac{87S_{\Gamma}}{86S_{\Gamma}})_{MORB} - (\frac{87S_{\Gamma}}{86S_{\Gamma}})_{T_{0}} - (\frac{87Rb}{86S_{\Gamma}})_{PM}(e^{\lambda_{87}T_{0}} - e^{\lambda_{87}T_{d}})}{(\frac{87Rb}{86S_{\Gamma}})_{PM}(e^{\lambda_{87}T_{d}} - 1)}, \quad (7)$$

$$z = \frac{1}{(X_{Sm} - X_{Nd})} \times \ln \frac{(\frac{143}{144}Nd}{(\frac{144}Nd})_{MORB} - (\frac{143}{144}Nd})_{T_{0}} - (\frac{147Sm}{144Nd})_{PM}(e^{\lambda_{147}T_{0}} - e^{\lambda_{147}T_{d}})}{(\frac{147}{144}Nd})_{PM}(e^{\lambda_{176}T_{d}} - 1)}.$$

$$(8)$$

The above two equations are used to solve for $(T_{\rm d}, z)$ iteratively using a MatLab program (provided in Supplementary File 1). Another way to solve for $(T_{\rm d}, z)$ is as follows: Calculate and plot z

for a given age $T_{\rm d}$ using Eq. (7) to obtain one z versus $T_{\rm d}$ curve, and using Eq. (8) to obtain another z versus $T_{\rm d}$ curve. The intersection of the two curves is the solution of model age of mantle depletion $T_{\rm d}$ and depletion factor z. Calculated examples will be given later.

Note that our model can only be applied to basalt from a depleted mantle source. It cannot be applied to basalt from an enriched mantle because the enrichment process is more complicated (mixing with various mantle components and/or metasomatism by mantle fluids and melts; Zindler and Hart, 1986; Hofmann, 2014).

3.2. Model assumptions, and reconciliation of two sets of CoI values

There are two assumptions in the model. The first assumption of the model is that a given piece of MORB mantle underwent a two-stage evolution, with the first stage in PM (i.e., with Rb/Sr and Sm/Nd ratio the same as those in PM) from age T_0 to age T_d , and the second stage in a specific DM from age T_d to age 0 (the present day). The recent (zero-age) depletion that led to MORB production does not affect the isotopic ratios. However, mantle depletion may be continuous or there may be multiple stages. Hence, T_d should in general be interpreted as an average depletion age (similar to a closure age). There may also be various kinds of mantle mixing (such as mixing between DMM and other mantle endmembers, or both pyroxenite and peridotite contributing to mantle partial melting) and metasomatism by fluids or small-degree melts, which would obscure the meanings of the calculated depletion age and depletion factor.

The second assumption is that the composition of a specific depleted mantle is related to a reference mantle by Eq. (4), that is, $\ln(C_{i,DM}/C_{i,PM})$ is proportional to $X_i = \text{CoI}_i$ (Zhang, 2014). We take advantage of two independently evaluated RDM compositions (Salters and Stracke, 2004; Workman and Hart, 2005) to check this assumption. These two RDM compositions are different and may be viewed as differently depleted mantle. If our second assumption holds, a plot of CoI values calculated in Zhang (2014) for the RDM of Workman and Hart (2005), which equals $ln(C_{i,RDM2}/C_{i,PM}) = CoI_{i,2}$, versus those of Salters and Stracke (2004), which equals $ln(C_{i,RDM1}/C_{i,PM}) = Col_{i,1}$, should be a straight line passing through the origin (0,0). Fig. 1 plots CoI values (Zhang, 2014) of RDM2 versus those of RDM1. The two sets of CoI values show an excellent proportionality relation, meaning that RDM2 has a single z value relative to RDM1, and vice versa. That is, Fig. 1 may be viewed as a validation of Eq. (4), because Eq. (4) essentially assumes that other specific depleted mantle also follows a similar relation.

When solving for (T_d, z) from $(^{87}Sr)^{86}Sr, ^{143}Nd)^{144}Nd)$ using Eqs. (7) and (8), using CoI values from Salters and Stracke (2004) would lead to one set of (T_d, z) using RDM1, and using CoI values from Workman and Hart (2005) would lead to a different set of (T_d, z) using RDM2. Note that T_d as the mantle depletion age is a physical parameter that should be independent of the adopted reference mantle composition. The different T_d values using RDM1 versus RDM2 are due to small errors (inconsistencies) in estimated compositions of RDM1 and RDM2. Realizing that CoI values using RDM2 and those using RDM1 are proportionally correlated within error (Fig. 1), we fit the data by y = ax using the York (1969) algorithm to account for errors and remove the inconsistency. The slope $a=1.341\pm0.096$. The mean square weighted deviation (MSWD) of the fit is 0.283, much smaller than 1, suggesting excellent fit. The fit also allows us to obtain adjusted CoI values for RDM1 and RDM2, and hence the adjusted concentrations for elements in RDM1 and RDM2 (C_{RDM1} and C_{RDM2}). The adjusted CoI_{RDM1}, CoI_{RDM2}, C_{RDM1}, and C_{RDM2} values are listed in Table 1 (bold), and are used to calculate mantle depletion ages and depletion factors so that our model calculation using any of

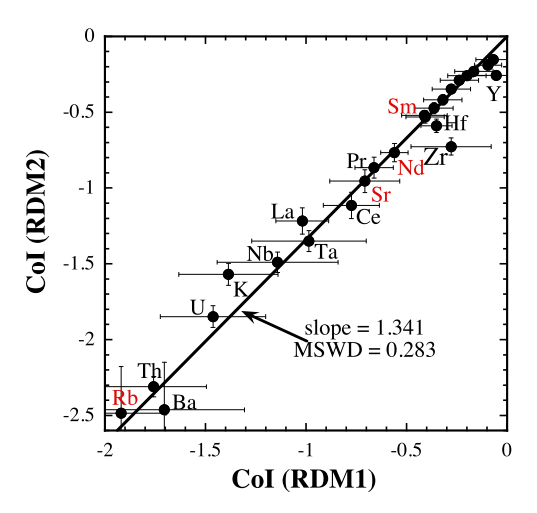


Fig. 1. Correlation between two sets of CoI values, showing that Eq. (4) holds for the more depleted mantle of Workman and Hart (2005) when compared to the RDM of Salters and Stracke (2004). The 1σ error bars are from Salters and Stracke (2004) and Workman and Hart (2005). 1σ error for RDM2 (Workman and Hart, 2005) is not directly given and we interpret the maximum concentration value in Workman and Hart (2005) to be $C_{\text{mean}} + 2\sigma$, and the minimum $= C_{\text{mean}} - 2\sigma$, leading to 1σ on CoI = $0.25 \cdot \ln(C_{\text{max}}/C_{\text{min}})$. CoI values (and concentrations) of all elements except Zr are well reconciled by the linear relation within error.

the two RDMs would generate the same $T_{\rm d}$. Although the z value still depends on the specific RDM ($z_2=z_1/1.341$), zX_i (where X_i is CoI of element i) will be independent of the RDM, meaning that the inferred mantle composition using Eq. (4) is independent of the RDM used.

In addition to the above two reference depleted mantle compositions, other depleted mantle compositions are possible. Calculated depleted MORB mantle compositions corresponding to different degrees of the depletion factor z are listed in Supplementary data file Table S2. For example, a depleted MORB mantle containing 10 ppb U (Langmuir, personal communication) corresponds to a z value of \sim 0.5, and that containing 8 ppb U (McDonough, personal communication) corresponds to a z value of \sim 0.67.

3.3. Various sources of uncertainties in the calculated model depletion age and depletion factor

There are a number of contributing factors to the uncertainties in the calculated ($T_{\rm d}$, z). Some uncertainty in ($T_{\rm d}$, z) are due to uncertainties in the input parameters: the age of the solar system T_0 (based on CAI age 4567.30 ± 0.16 Ma, Connelly et al., 2012), the atomic ratio ($^{147}{\rm Sm}/^{144}{\rm Nd})_{\rm PM}=0.1960\pm0.0004$ (Jacobsen and Wasserburg, 1984; Bouvier et al., 2008), the present day $^{143}{\rm Nd}/^{144}{\rm Nd}=0.512630\pm0.000011$ (Bouvier et al., 2008), the initial ratio ($^{87}{\rm Sr}/^{86}{\rm Sr})_{T_0}=0.69877\pm0.00001$ (Gray and Wasserburg, 1973), the atomic ratio ($^{87}{\rm Rb}/^{86}{\rm Sr})_{\rm PM}$, and the uncertainty in measured $^{87}{\rm Sr}/^{86}{\rm Sr}$ and $^{143}{\rm Nd}/^{144}{\rm Nd}$ ratios in a given MORB sample. The uncertainties in calculated ($T_{\rm d}$, z) due to small errors in T_0 , ($^{147}{\rm Sm}/^{144}{\rm Nd})_{\rm PM}$, ($^{143}{\rm Nd}/^{144}{\rm Nd})_{\rm PM}$, and ($^{87}{\rm Sr}/^{86}{\rm Sr})_{T_0}$ are insignificant.

Among the parameters, the atomic ratio (87 Rb/ 86 Sr)_{PM} has the largest relative uncertainty, 0.0873 \pm 0.0276 by McDonough and Sun (1995), 0.0863 \pm 0.0122 by Palme and O'Neill (2004), and 0.0796 \pm 0.0089 by Palme and O'Neil (2014). Trial calculations show that the (87 Rb/ 86 Sr)_{PM} ratio affects the calculated (T_d , z) significantly. Table S3 shows an example of how T_d would decrease and z would increase when the assumed (87 Rb/ 86 Sr)_{PM} ratio decreases.

To choose the best $(^{87}\text{Rb}/^{86}\text{Sr})_{PM}$ ratio for our model, we show calculated $(T_{\rm d},z)$ values for all the isotope data in MORB that satisfy the criteria $^{87}\text{Sr}/^{86}\text{Sr} < 0.70452$ and $^{143}\text{Nd}/^{144}\text{Nd} > 0.51263$ in Fig. 2 by varying $(^{87}\text{Rb}/^{86}\text{Sr})_{PM}$ ratio. It can be seen that most

Table 1 Adjusted Col values compared to Col values in Zhang (2014).

Element	CoI(RDM1) Ref. 1	Col _{RDM1} adjusted	C_{RDM1} adjusted	CoI(RDM2) Ref. 1	Col _{RDM2} adjusted	C_{RDM2} adjusted
Rb	-1.920	-1.888	0.091	-2.485	-2.531	0.0477
Ba	-1.705	-1.803	1.09	-2.462	-2.417	0.589
Th	-1.758	-1.723	0.0142	-2.309	-2.311	0.00789
U	-1.463	-1.381	0.00510	-1.847	-1.852	0.00319
K	-1.386	-1.180	73.8	-1.569	-1.582	49.3
Nb	-1.142	-1.111	0.217	-1.489	-1.490	0.148
Ta	-0.986	-1.005	0.0135	-1.349	-1.348	0.0096
La	-1.019	-0.929	0.256	-1.216	-1.245	0.187
Ce	-0.775	-0.821	0.737	-1.114	-1.101	0.557
Sr	-0.708	-0.711	9.77	-0.954	-0.954	7.67
Pr	-0.662	-0.649	0.133	-0.865	-0.870	0.106
Nd	-0.561	-0.568	0.708	-0.766*	-0.762	0.584
Zr	-0.279	-0.530	6.18	-0.726	-0.711	5.16
Hf	-0.352	-0.425	0.185	-0.589	-0.570	0.160
Sm	-0.408	-0.396	0.273	-0.530	-0.532	0.239
Ti	-0.412	-0.389	817	-0.520	-0.521	715
Eu	-0.364	-0.354	0.108	-0.473	-0.474	0.096
Gd	-0.320	-0.312	0.398	-0.418	-0.419	0.358
Tb	-0.278	-0.260	0.0764	-0.347	-0.348	0.0699
Dy	-0.238	-0.216	0.543	-0.289	-0.290	0.504
Но	-0.200	-0.193	0.123	-0.259	-0.259	0.115
Y	-0.055	-0.189	3.56	-0.256	-0.253	3.34
Er	-0.166	-0.171	0.369	-0.230	-0.230	0.348
Yb	-0.095	-0.140	0.383	-0.189	-0.187	0.366
Lu	-0.069	-0.113	0.0603	-0.152	-0.151	0.0580

Ref. 1 means Zhang (2014). RDM1 stands for the reference depleted mantle of Salters and Stracke (2004), and RDM2 stands for the reference depleted mantle of Workman and Hart (2005). C_{RDM1} and C_{RDM2} are concentrations of elements in ppm in RDM1 and RDM2.

^{*} This corrects a typographical error in Zhang (2014).

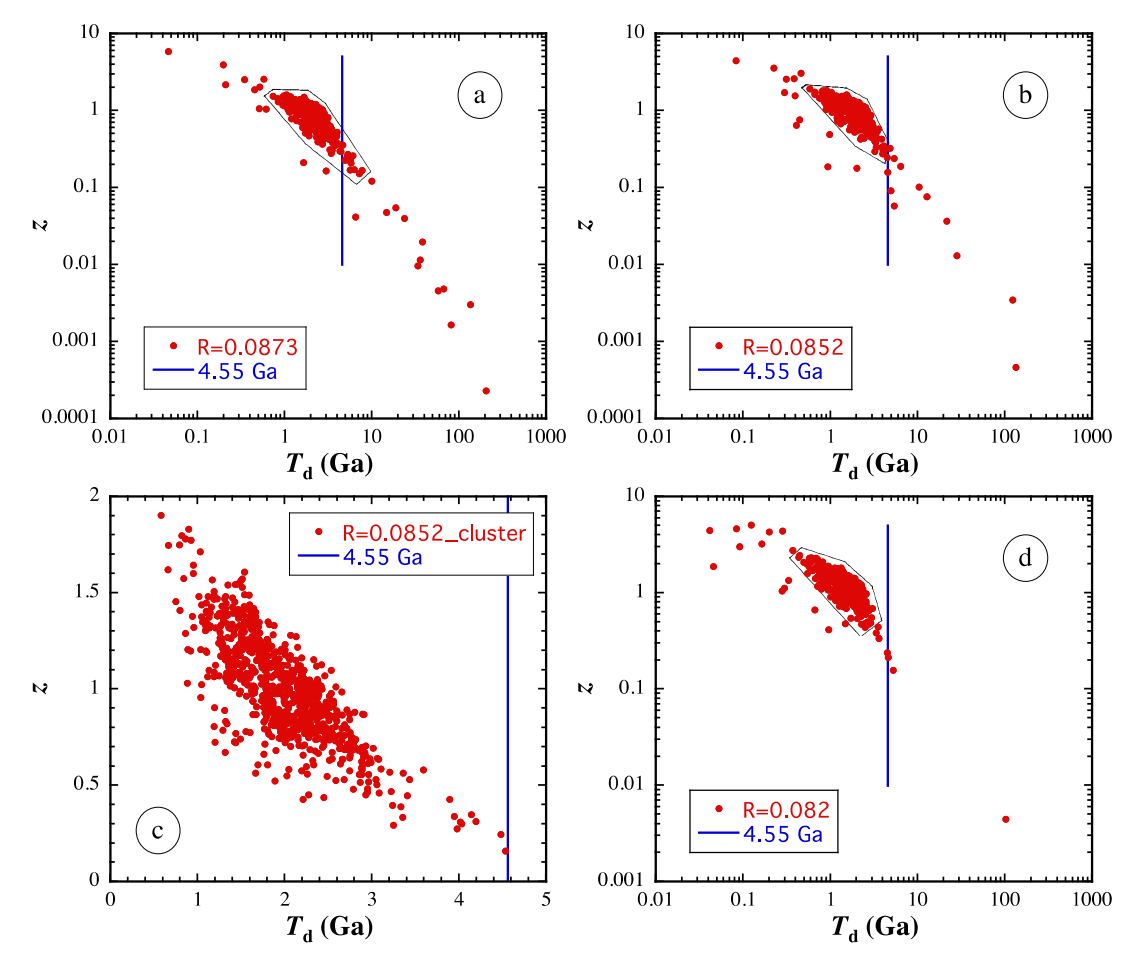


Fig. 2. The depletion factor z versus the depletion age T_d in Ga calculated for 895 pairs of Sr-Nd isotope data using different $R = (^{87}\text{Rb})^{86}\text{Sr})_{PM}$ values. Most of the results are in a cluster (outlined) in z versus T_d plot. When R = 0.0852, the oldest age of the cluster is \sim 4.55 Ga. (c) is an enlargement of (b) showing only the data in the cluster. Note that (c) is in linear scale and other panels are in logarithm scale. (For interpretation of the colors in the figure(s), the reader is referred to the web version of this article.)

(97.1%) of the 895 data points plot as a cluster (outlined by thin blue segments in Fig. 2a, b and d). A value of $(^{87}\text{Rb}/^{86}\text{Sr})_{PM}=0.0852$ is chosen for our model calculations so that the maximum age of the cluster is about 4.55 Ga (vertical blue line in Fig. 2). This value of $(^{87}\text{Rb}/^{86}\text{Sr})_{PM}=0.0852$ is between the values of McDonough and Sun (1995) and Palme and O'Neil (2014). The 26 data points (2.9% of the Sr-Nd isotope data) resulting in $(T_{\rm d}, z)$ values outside the outlined cluster are treated as outliers and not used further.

Another uncertainty is on the timing from chondritic elemental ratios to PM elemental ratios. It is possible that terrestrial material acquired the ratio $(^{87}\text{Rb}/^{86}\text{Sr})_{PM}$ at an age of T_{0a} that is slightly younger than T_0 . For example, ${}^{87}\text{Sr}/{}^{86}\text{Sr}$ ratio might have evolved in a reservoir with (87Rb/86Sr)_{CHON} (where subscript CHON means chondritic) ratio from T_0 (4.5673 Ga) to T_{0a} (e.g., 4.560 Ga), and then in a reservoir with (87Rb/86Sr)_{PM} ratio from T_{0a} to T_d . The timing of T_{0a} would not affect the Sm-Nd system because $(^{147}\text{Sm}/^{144}\text{Nd})_{\text{PM}} = (^{147}\text{Sm}/^{144}\text{Nd})_{\text{CHON}}$. However, the timing would affect the Rb-Sr system significantly because $(^{87}\text{Rb}/^{86}\text{Sr})_{\text{CHON}} \approx 10(^{87}\text{Rb}/^{86}\text{Sr})_{\text{PM}}$ (McDonough and Sun, 1995; Palme and O'Neill, 2004; 2014). As T_{0a} becomes younger than T_0 , T_d would increase and z would decrease; an example is given in Table S4. Because there is currently no constraint on T_{0a} , in this work the default is $T_{0a} = T_0$. That is, $(^{87}\text{Rb})^{86}\text{Sr}$) is the same as (87Rb/86Sr)_{PM} from 4.5673 Ga until mantle depletion. Future research may reveal that terrestrial materials evolved in chondritic environment (meaning $^{87}\text{Rb}/^{86}\text{Sr} = (^{87}\text{Rb}/^{86}\text{Sr})_{\text{CHON}} \approx 0.9)$ for a short period of time (such as 5 or 10 Myr) and then in the PM environment (meaning 87 Rb/ 86 Sr = (87 Rb/ 86 Sr)_{PM}). If so, our model would have to be updated using new T_{0a} as well as new (87Rb/86Sr)_{PM} determined using a similar approach as Fig. 2.

Measured 87 Sr/ 86 Sr and 143 Nd/ 144 Nd ratios in MORB also have uncertainties. When $T_{\rm d}$ and z are solved from 87 Sr/ 86 Sr and 143 Nd/ 144 Nd ratios, uncertainties in $T_{\rm d}$ and z are correlated and can be obtained from errors in 87 Sr/ 86 Sr and 143 Nd/ 144 Nd ratios. Because the compilation in Gale et al. (2013) did not include errors for the isotope ratios, we adopt a typical 1σ error of 0.00001 for measured 87 Sr/ 86 Sr ratio and 143 Nd/ 144 Nd ratio, and a 1σ error of 0.000005 for measured 176 Hf/ 177 Hf ratio. The resulting 1σ uncertainties on ($T_{\rm d}$, z) are correlated and better represented by a parallelogram than by mutually perpendicular error bars (Fig. 3).

In summary, due to uncertainty in the various input parameters, there is large uncertainty in the absolute values of the calculated depletion ages as well as the depletion factors. The relative ages (which MORB source is older and which MORB source is younger) and relative depletion factors are more reliable.

In addition to uncertainties in the input parameters, processes that can affect the isotope ratios of a MORB would result in additional errors. These processes include pyroxenite contribution to a specific MORB (Stracke et al., 1999), mixing of enriched mantle into the MORB mantle source, and metasomatism by mantle fluids and low-degree partial melts. If the effect on the Sr-Nd isotopes is quantifiable, then the error on the calculated depletion age and factor can also be quantified.

3.4. A numerical example of model application

We show a numerical example of applying our model to a specific MORB here to help readers who are interested in carrying out similar calculations. The example is for a mid-Atlantic ridge basalt sample END0025-006-003, with 87 Sr/ 86 Sr = 0.702710; 143 Nd/ 144 Nd = 0.513135; and 176 Hf/ 177 Hf = 0.283279 (Gale et al., 2013). Fig. 4 shows the calculated z- $T_{\rm d}$ curves using Eqs. (7) and (8). The calculated z- $T_{\rm d}$ curve to satisfy (87 Sr/ 86 Sr) = 0.702710 using Eq. (7) is shown as a solid red curve, and that to satisfy (143 Nd/ 144 Nd) = 0.513135 using Eq. (8) is shown as a dashed

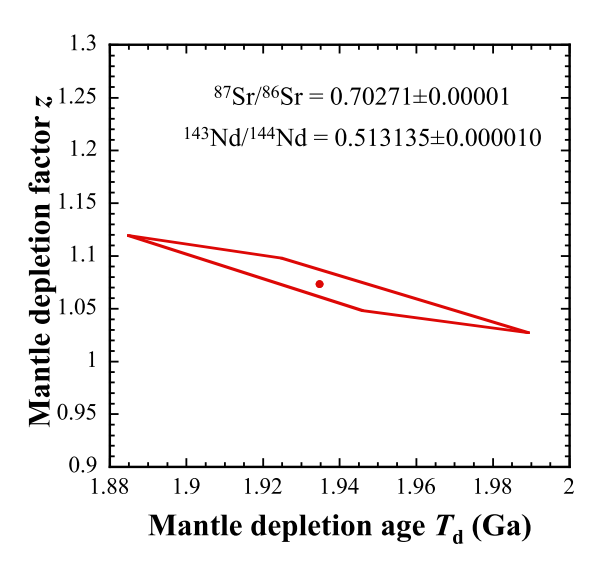


Fig. 3. Error on calculated $T_{\rm d}$ and z for the data with 0.00001 as 1σ errors on $^{87}{\rm Sr}/^{86}{\rm Sr}$ and $^{143}{\rm Nd}/^{144}{\rm Nd}$ ratios. The errors on z and $T_{\rm d}$ are correlated. Hence, displaying simple horizontal and vertical error bars is not the most informative. The error parallelograms as shown here are a better representation of the errors.

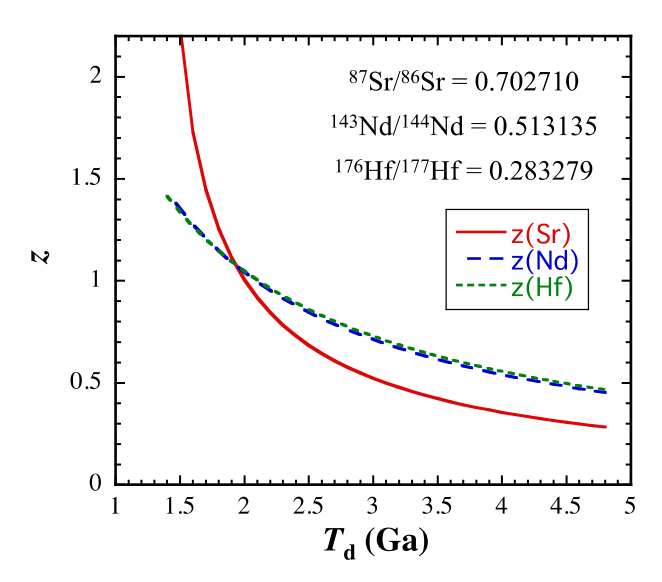


Fig. 4. Graphical method to find the solution of mantle depletion factor and depletion age at the intersection of two curves using Sr-Nd isotopes. One may also use Sr-Nd-Hf isotopes. Then, if all three isotope-ratios have no errors and are perfectly consistent with the model, all three curves would intersect at one point. RDM1 is used as the reference depleted mantle. Based on Sr-Nd isotopes, $T_{\rm d}=1.93$ Ga, and z=1.07. The age using RDM2 as reference is the same as that using RDM1 but the depletion factor is 1.07/1.341=0.80. The blue dashed curve (based on $^{148}{\rm Nd}/^{144}{\rm Nd}$ ratio) is subparallel with the green short-dashed curve (based on $^{176}{\rm Hf}/^{177}{\rm Hf}$, meaning that $^{176}{\rm Hf}/^{177}{\rm Hf}$ does not provide much additional constraint on the mantle depletion $T_{\rm d}$ or z.

blue curve. (The green short-dashed curve for 176 Hf/ 177 Hf will be discussed later.) The solution for $T_{\rm d}$ and z is at the intersection of the solid red curve and the dashed blue curve, leading to $T_{\rm d}=1.93$ Ga and z=1.07. This calculation uses RDM1 as the reference depleted mantle. If RDM2 is used, then $T_{\rm d}$ is the same but z=1.07/1.341=0.80. Once $T_{\rm d}$ and z are solved from Sr-Nd isotope ratios, isotope evolution of the mantle source of the specific MORB sample END0025-006-003 in the context of our two-stage evolution model can be calculated as shown in Fig. S1.

Furthermore, trace element concentrations of the mantle source prior to the production of this MORB END0025-006-003 can also be calculated using Eq. (4) based on z=1.07 and adjusted Col values for RDM1 (Table 1). The results are shown in Table 2. The

Table 2 Inferred trace element concentrations (ppm) in the mantle source of MAR(END0025-006-003).

Element	Rb	Ba	Th	U	Nb	Ta	La	Ce	Sr	Pr	Nd	Zr
C_i^0	0.079	0.95	0.0125	0.0046	0.200	0.0126	0.239	0.694	9.28	0.127	0.679	5.94
C_i^{melt}	1.68	19.9	0.194	0.069	3.39	0.196	2.71	7.75	79.7	1.303	6.958	66.5
C_i^{melt}/C_i^0	21.24	20.9	15.5	15.0	17.0	15.6	11.3	11.2	8.59	10.3	10.2	11.2
Element	Hf	Sm	Ti	Eu	Gd	Tb	Dy	Но	Y	Er	Yb	Lu
C_i^0	0.179	0.265	794	0.105	0.389	0.075	0.534	0.121	3.51	0.364	0.380	0.060
C melt	1.86	2.67	7656	0.961	3.66	0.701	4.85	1.063	31	3.19	3.12	0.481
				9.12	9.41	9.36	9.07	8.78	8.83	8.75	8.22	8.04

 C_i^0 is the inferred mantle source composition prior to MORB production using Eq. (4). C_i^{melt} is the composition of this MORB sample (Gale et al., 2013).

inferred composition of the depleted mantle source (C_i^0 in Table 2) in this work are highly correlated with the measured MORB composition (C_i^{melt} in Table 2) given in Gale et al. (2013), and the ratio C_i^{melt}/C_i^0 is well correlated with bulk partition coefficient listed in Workman and Hart (2005), which supports the validity of the inferred MORB source mantle composition. Theoretically, knowing the specific source mantle composition, the degree of partial melting of the specific MORB may be inferred. However, using either a batch melting model or a fractional melting model (Shaw, 1970) with constant partition coefficients in Workman and Hart (2005) cannot reproduce the trace element pattern in MORB to within about 20%. We interpret the results (the inability to reproduce MORB composition by either batch melting or fractional melting) to mean that the partial melting process that produced the sample END0025-006-003 is more complicated (e.g., Langmuir et al., 1977), or partition coefficients are variable along the melting column (Shaw, 1970). However, inaccuracy of the partition coefficients or the inferred source composition may also lead to mismatch in modeled versus observed MORB composition. Nonetheless, the ability to estimate the composition of the mantle source will facilitate modeling of mantle partial melting process that produced MORB.

3.5. Use of Hf and Pb isotope ratios

Theoretically, other isotope ratios can also be used to estimate the mantle depletion age and depletion factor. Because there are only two unknowns, when more than two isotope ratios are used, in principle, nonlinear regression method may be applied to obtain the best (least-squares) solution for $T_{\rm d}$ and z, meaning that mantle depletion ages would be better constrained. Or alternatively, more isotope data might allow multiple depletion events to be constrained. We first consider $^{176}{\rm Hf}/^{177}{\rm Hf}$ isotope ratios, and z versus $T_{\rm d}$ equation for $^{176}{\rm Hf}/^{177}{\rm Hf}$ ratio can be readily written by analogy to Eq. (8) as follows:

$$z = \frac{1}{(X_{\text{Lu}} - X_{\text{Hf}})} \times \ln \frac{(\frac{^{176}\text{Hf}}{^{177}\text{Hf}})_{\text{MORB}} - (\frac{^{176}\text{Hf}}{^{177}\text{Hf}})_{T_0} - (\frac{^{176}\text{Lu}}{^{177}\text{Hf}})_{\text{PM}} (e^{\lambda_{176}T_0} - e^{\lambda_{176}T_d})}{(\frac{^{176}\text{Lu}}{^{177}\text{Hf}})_{\text{PM}} (e^{\lambda_{176}T_d} - 1)},$$
(9

where $(^{176}\text{Lu}/^{177}\text{Hf})_{PM} = 0.0336\pm0.0001$ (Bouvier et al., 2008), $\lambda_{176} = 0.01867\pm0.00007$ By $^{-1}$ (Bouvier et al., 2008), $(^{176}\text{Hf}/^{177}\text{Hf})_{T_0} = 0.282785\pm0.000011$ (Bouvier et al., 2008), and $X_{\text{Lu}} - X_{\text{Hf}} = 0.3125$ (Table 1). $^{176}\text{Hf}/^{177}\text{Hf}$ and $^{143}\text{Nd}/^{144}\text{Nd}$ isotope ratios are typically linearly correlated (Patchett, 1983; Bouvier et al., 2008) but significant decoupling between $^{176}\text{Hf}/^{177}\text{Hf}$ and $^{143}\text{Nd}/^{144}\text{Nd}$ have been observed (Salters et al., 2011; Stracke et al., 2011). Fig. 4 shows a typical z versus T_{d} curve for $^{176}\text{Hf}/^{177}\text{Hf}$ (green

short dashes), which is subparallel with and nearly identical to that for ¹⁴³Nd/¹⁴⁴Nd (blue dashes). In such cases, the ¹⁷⁶Hf/¹⁷⁷Hf ratio essentially does not provide much additional constraint on T_d and z. If Nd-Hf isotopes were used to calculate mantle depletion age, the results would be two subparallel and nearly identical trends as in Fig. 4: often there is no solution for (T_d, z) ; and if there is a solution (i.e., intersection of the two subparallel curves), the errors would be much larger compared to the calculation using Sr-Nd isotope ratios. On the other hand, it is possible to use ${}^{87}\mathrm{Sr}/{}^{86}\mathrm{Sr}-{}^{176}\mathrm{Hf}/{}^{177}\mathrm{Hf}$ isotope ratios to estimate T_d and z, and the results would have similar or smaller uncertainties compared to using ${}^{87}\mathrm{Sr}/{}^{86}\mathrm{Sr}-{}^{143}\mathrm{Nd}/{}^{144}\mathrm{Nd}$ isotope ratios. However, there are only 309 MORB samples with both 87 Sr/ 86 Sr and 176 Hf/ 177 Hf data, only 260 samples with ⁸⁷Sr/⁸⁶Sr-¹⁴³Nd/¹⁴⁴Nd-¹⁷⁶Hf/¹⁷⁷Hf data, compared to 869 MORB samples with ⁸⁷Sr/⁸⁶Sr and ¹⁴³Nd/¹⁴⁴Nd data. Calculated mantle depletion ages using 87 Sr/ 86 Sr- 176 Hf/ 177 Hf isotope ratios are compared with those using 87 Sr/ 86 Sr- 143 Nd/ 144 Nd isotope ratios in Fig. S2. To the first order, mantle depletion ages from Sr-Hf isotopes are similar to those from Sr-Nd isotope ratios (Fig. S2). However, if the ¹⁷⁶Hf/¹⁷⁷Hf ratio is significantly above the average ¹⁷⁶Hf/¹⁷⁷Hf versus 143Nd/144Nd trend (such as Knipovich Ridge, Salters et al., 2011), the calculated age based on Sr-Hf isotopes would be noticeably younger (e.g., by 0.2 Ga) than that based on Sr-Nd age. Conversely, if the ¹⁷⁶Hf/¹⁷⁷Hf ratio is significantly below the average ¹⁷⁶Hf/¹⁷⁷Hf versus ¹⁴³Nd/¹⁴⁴Nd trend (such as East Pacific Rise, Salters et al., 2011), the calculated age based on Sr-Hf isotopes would be significantly older than that based on Sr-Nd age. Such inconsistency might be due to processes other than the twostage mantle evolution modeled here, such as those discussed by Salters et al. (2011). Our discussion below will focus on results from the larger dataset of ⁸⁷Sr/⁸⁶Sr-¹⁴³Nd/¹⁴⁴Nd isotopes.

For Pb isotope ratios, there are three ratios in U-Th-Pb system, and two ratios from U-Pb system. Hence, in principle, they may provide major constraints. However, there are at least two difficulties. One difficulty is that the ratios in PM are not known. For example, Halliday (2004) listed 11 sets of estimated Pb isotope ratios in the bulk silicate Earth or primitive mantle. When these were adopted, very different ages would result from the 11 different estimates. The other difficulty is that Pb concentrations in MORB cannot be accounted for by melt depletion alone; there seems to be depletion of Pb complementary to the continental crust acquired early in Earth history (Hofmann, 2014). Therefore, Pb isotope ratios are not used here.

3.6. Extension of the model to non-zero-age depleted basalts

The set of equations given above are for zero-age MORBs. Our model can be readily extended to treat non-zero-age and unaltered MORB. To apply our model to non-zero-age depleted basalts, the first step is to calculate 87 Sr/ 86 Sr and 143 Nd/ 144 Nd ratios at the eruption age $T_{\rm e}$ (correcting for post-eruption isotope growth). Then Eqs. (1), (2), (7) and (8) can be modified as follows:

$$\left(\frac{^{87}\text{Sr}}{^{86}\text{Sr}}\right)_{T_{e}} = \left(\frac{^{87}\text{Sr}}{^{86}\text{Sr}}\right)_{T_{0}} + \left(\frac{^{87}\text{Rb}}{^{86}\text{Sr}}\right)_{PM} (e^{\lambda_{87}T_{0}} - e^{\lambda_{87}T_{d}}) + \left(\frac{^{87}\text{Rb}}{^{86}\text{Sr}}\right)_{DM} (e^{\lambda_{87}T_{d}} - e^{\lambda_{87}T_{e}}), \tag{1}''$$

$$\begin{split} \left(\frac{^{143}\text{Nd}}{^{144}\text{Nd}}\right)_{T_e} &= \left(\frac{^{143}\text{Nd}}{^{144}\text{Nd}}\right)_{T_0} + \left(\frac{^{147}\text{Sm}}{^{144}\text{Nd}}\right)_{PM} (e^{\lambda_{147}T_0} - e^{\lambda_{147}T_d}) \\ &+ \left(\frac{^{147}\text{Sm}}{^{144}\text{Nd}}\right)_{DM} (e^{\lambda_{147}T_d} - e^{\lambda_{147}T_e}), \end{split} \tag{2}$$

$$z = \frac{1}{(X_{Rb} - X_{Sr})} \times \ln \frac{(\frac{^{87}Sr}{^{86}Sr})_{T_e} - (\frac{^{87}Sr}{^{86}Sr})_{T_0} - (\frac{^{87}Rb}{^{86}Sr})_{PM}(e^{\lambda_{87}T_0} - e^{\lambda_{87}T_d})}{(\frac{^{87}Rb}{^{86}Sr})_{PM}(e^{\lambda_{87}T_d} - e^{\lambda_{87}T_e})},$$
(7)

$$z = \frac{1}{(X_{\text{Sm}} - X_{\text{Nd}})} \times \ln \frac{(\frac{143 \text{ Nd}}{144 \text{ Nd}})_{T_e} - (\frac{143 \text{ Nd}}{144 \text{ Nd}})_{T_0} - (\frac{147 \text{ Sm}}{144 \text{ Nd}})_{PM} (e^{\lambda_{147} T_0} - e^{\lambda_{147} T_d})}{(\frac{147 \text{ Sm}}{144 \text{ Nd}})_{PM} (e^{\lambda_{176} T_d} - e^{\lambda_{147} T_e})}.$$
(8')

The mantle depletion age T_d and the depletion factor z can then be solved from Eqs. (7') and (8').

4. Model applications and discussion

One specific application is to infer the mantle source composition of a specific MORB (Table 2), which has already been presented in Section 3.4. Once the mantle depletion age and factor for a given MORB is calculated using our model, the isotope evolution history of the specific mantle source can also be inferred (Fig. S1). Furthermore, the incompatible trace element pattern of the mantle source prior to the recent MORB production can be combined with the measured MORB composition to investigate mantle partial melting process that generated the MORB.

In this section, we apply the model to the global MORB database on Sr and Nd isotopes (Supplementary Table S1). Due to sensitivity of the calculated mantle depletion age (T_d) and depletion factor (z) on some input parameters (especially $(^{87}\text{Rb})^{86}\text{Sr})_{PM}$ and T_{a0} , see Section 3) and uncertainties in constraining them, the absolute values of the calculated mantle depletion age and depletion factor are less reliable, but the relative values (which source has an older depletion age versus which has a younger age) are more reliable. Calculated mantle source depletion age and depletion factor relative to RDM1 for all available MORB data are shown in Fig. 5. A depletion factor (z) of 1 means that the given mantle source has the same composition as the RDM used. If RDM2 is used as the reference depleted mantle, the calculated mantle depletion age and calculated mantle source composition are the same but the depletion factor z (which is relative to a given reference depleted mantle) would differ by a factor of 1.341 (see Section 3).

Based on results shown by Fig. 5 (also Fig. 2c), sub-ridge mantle depletion age ranges from 0.5 to 4.5 Ga (the upper limit of 4.5 Ga is due to our choice of $(^{87}\text{Rb}/^{86}\text{Sr})_{PM}$ and isotope data). Both the absolute and relative uncertainties in $T_{\rm d}$ (using 1σ error of 10^{-5} for both $^{87}\text{Sr}/^{86}\text{Sr}$ and $^{143}\text{Nd}/^{144}\text{Nd}$ ratios) increase as $T_{\rm d}$ increases. When the calculated age is >4.0 Ga, the 1σ error in the calculated age is often >1.0 Ga. The mantle depletion factor ranges from 0.15 to 1.95 relative to RDM1. The uncertainty in z is 0.08 to 0.2, roughly independent of the value of z. The average depletion age

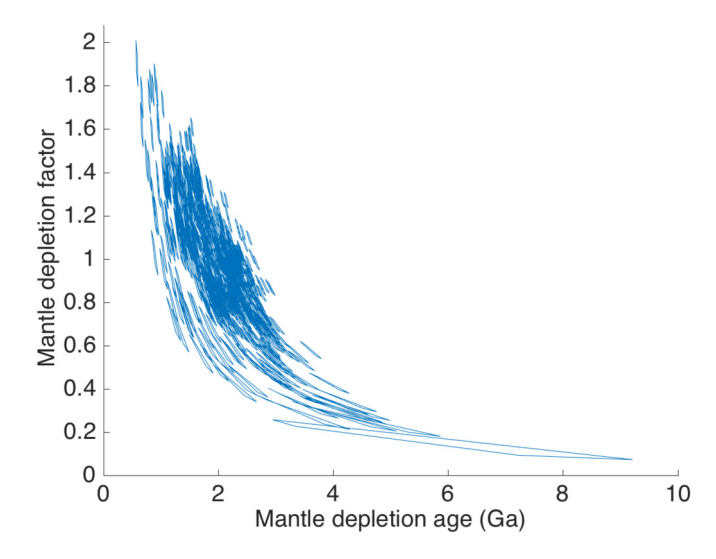


Fig. 5. Calculated sub-ridge mantle depletion factor versus depletion age based on ${}^{87}\mathrm{Sr}/{}^{86}\mathrm{Sr}$ and ${}^{143}\mathrm{Nd}/{}^{144}\mathrm{Nd}$ ratios in MORB. Every "point" is shown as a parallelogram that includes the 1σ uncertainty by assuming the measurement error in each of the ${}^{87}\mathrm{Sr}/{}^{86}\mathrm{Sr}$ and ${}^{143}\mathrm{Nd}/{}^{144}\mathrm{Nd}$ ratios is 0.00001. The mantle depletion factor z is defined in Eq. (4) with X_i being Col values relative to RDM1. (${}^{87}\mathrm{Rb}/{}^{86}\mathrm{Sr}/{}_{\mathrm{PM}} = 0.0852$ (see Section 3) and $T_{0a} = T_0 = 4.5673$ Ga (see Section 3).

of depleted MORB mantle sources is 1.983 Ga. The average depletion factor (z) when using RDM1 as the reference depleted mantle is 1.003, very close to 1, implying that RDM1 (Salters and Stracke, 2004) is very close to the average depleted MORB mantle (assuming the isotope ratios represent random samples). On the other hand, average z value of all depleted MORB mantle sources when RDM2 is used as the reference depleted mantle is 1.003/1.341 = 0.748, meaning that RDM2 (Workman and Hart, 2005) is significantly more depleted that the average depleted MORB mantle.

It is noteworthy that the model depletion age is inversely correlated with the depletion factor: when the model depletion age is old (e.g., older than 3.5 Ga), the depletion factor is low (Fig. 5). Observationally, this is due to the absence of very low 87 Sr/86 Sr and very high ¹⁴³Nd/¹⁴⁴Nd ratios. For example, if a domain of depleted mantle formed at 4.4 Ga (age of oldest detrital zircon, Wilde et al., 2001) and has the composition of RDM1 ($z_1 = 1$), the presentday isotope ratios in the depleted mantle would be: 87 Sr/86 Sr =0.700648, 143 Nd/ 144 Nd = 0.513702 ($\epsilon_{Nd} = +20.9$). Such extremely low 87 Sr/86 Sr ratio is not observed in MORB. On the other hand, smaller degrees of mantle depletion (small z values) during early Earth evolution are not expected because mantle temperature in Hadean is thought to be higher (e.g., Pollack, 1986; Condie, 2018) and hence the degree of partial melting should be higher, leading to greater degree of mantle depletion. The inconsistency between the expected higher degree of depletion and the inferred lower degree of depletion in early mantle partial melting implies a mantle depletion paradox. Possible explanations include: Early depleted mantle domains with high z values are not capable of generating MORB anymore so that they cannot be seen, or they were mixed with enriched mantle endmembers or subducted rocks (such as garnet pyroxenites) or low-degree melts/fluids in the long history of mantle convection.

Fig. 6 shows calculated mantle depletion ages in terms of Sr-Nd isotope ratios. It can be seen that at the same 87 Sr/ 86 Sr, smaller 143 Nd/ 144 Nd leads to older mantle depletion ages; at the same 143 Nd/ 144 Nd, smaller 87 Sr/ 86 Sr leads to older mantle depletion ages. Furthermore, the mantle sources for isotopically the most depleted MORB (lowest 87 Sr/ 86 Sr and highest 143 Nd/ 144 Nd) in the database do not correspond to the oldest depletion ages, but have depletion ages of 2.0 to 3.0 Ga. Using Fig. 6, one may quickly estimate the mantle depletion age from Sr-Nd isotope ratios.

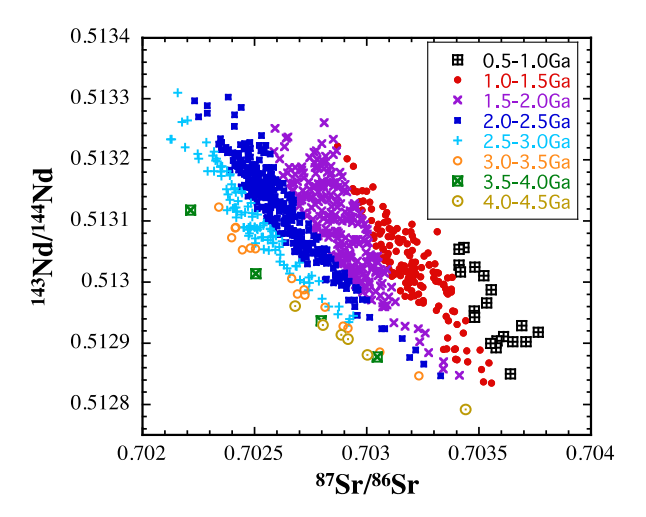


Fig. 6. Isotope ratio plot, using different symbols and colors to distinguish calculated model ages of mantle depletion. $(^{87}\text{Rb})^{86}\text{Sr})_{PM}=0.0852$, and $T_{0a}=T_0=4.5673$ Ga (see Section 3).

Model mantle depletion ages of all, Atlantic, Indian and Pacific MORBs are shown as histograms in Fig. 7. Globally, most model ages of mantle depletion are between 0.8-3.0 Ga. The distribution of depletion age of all MORB mantle sources is unimodal but non-Gaussian with a peak at 2.3 Ga. The depletion age of the Atlantic sub-ridge mantle (including mantle beneath the Mohns-Knipovich ridge) displays a bimodal distribution, with a major peak at 1.7 Ga and a minor peak at 2.3 Ga. Pacific MORB mantle source depletion age exhibits a unimodal and narrow distribution, with a

single peak at 2.3 Ga. For Indian sub-ridge mantle domains, the model age distribution is unimodal with a single peak at 1.7 Ga.

There is general similarity but also significant difference between the histogram of our model mantle depletion ages for all sub-ridge mantles (Fig. 7a), that of Nd model ages for continental crust rocks (Moller et al., 1998), and that of Re-depletion ages (T_{RD}) from on and off craton peridotites (Hawkesworth et al., 2017). For example, the Nd model ages for continental crust rocks display a bimodal distribution with peaks at 1.7 and 2.7 Ga with a mean of 2.4 Ga (Moller et al., 1998; all data are plotted in Fig. S3 in Appendix), whereas MORB mantle depletion age distribution has a single peak at 2.3 Ga. On the other hand, the histograms of model ages of mantle depletion in this work are clearly different from the histogram of zircon formation ages (Hawkesworth et al., 2017), with the latter having distinct peaks at 2.7, 2.5, 2.0, 1.1, 0.55, 0.1-0.3 Ga. Hawkesworth et al. (2017) attributed the various peaks in the zircon ages to crustal reworking such as magmatic activities during supercontinent assembly, which are not directly related to mantle depletion. Furthermore, our sub-ridge mantle depletion ages based on MORB isotopes are clearly different from the Nd model ages based on Nd isotopes in abyssal peridotites, which range from 0 to 2.4 Ga with a peak at 0.3 Ga (Mallick et al., 2014). It is not clear why there is such large difference in mantle depletion ages between MORB and abyssal peridotites.

The global geographical distribution of mantle depletion ages is shown in Fig. 8. There are large-scale patterns. For example, the sub-ridge mantle source domains of Mid-Atlantic-Ridge basalts are relatively young (mostly 0.8 to 2.2 Ga) north of 30°N, then increases southward, reaching a very old age peak (>4.0 Ga) between 5°N and 1°S, then decreases to 2.0 to 3.0 Ga between 5°S to 42°S, and then a mixture of young and old ages south of 42°S.

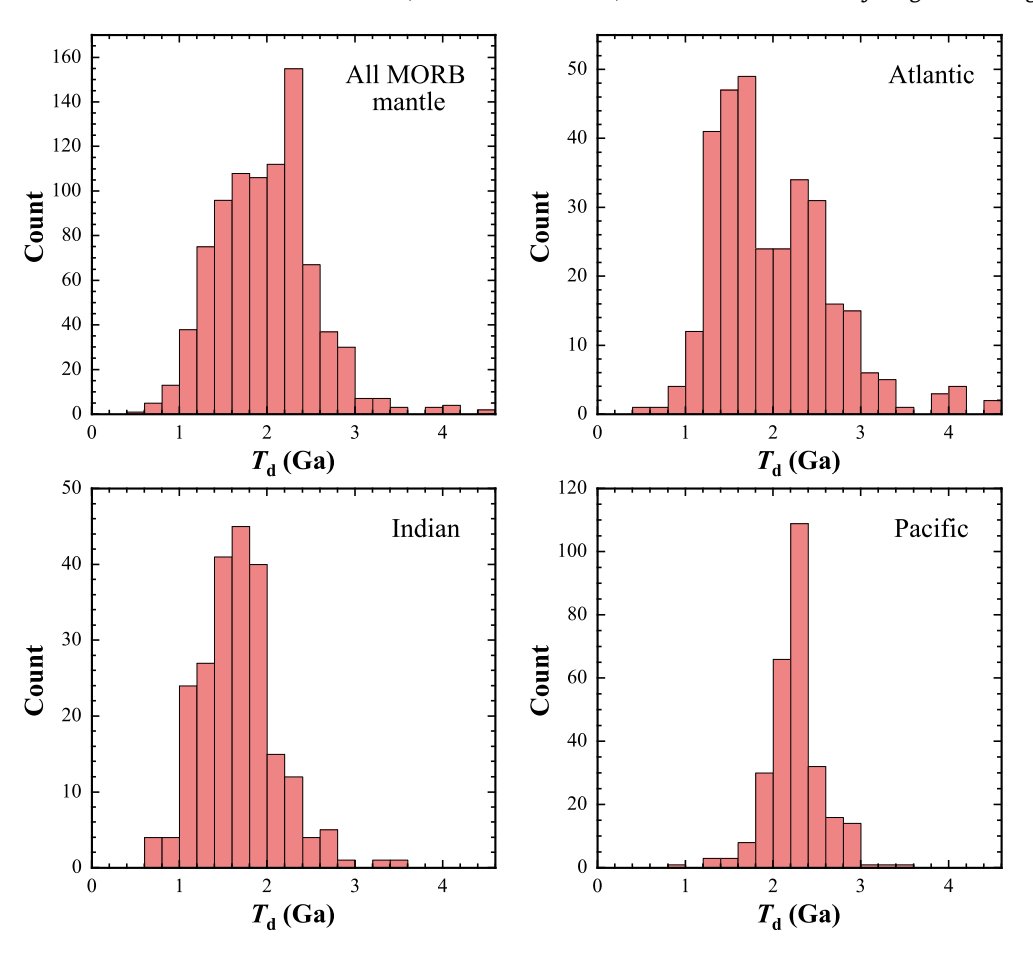


Fig. 7. Histogram of mantle source age of MORBs from different oceans. $(^{87}\text{Rb}/^{86}\text{Sr})_{PM} = 0.0852$.

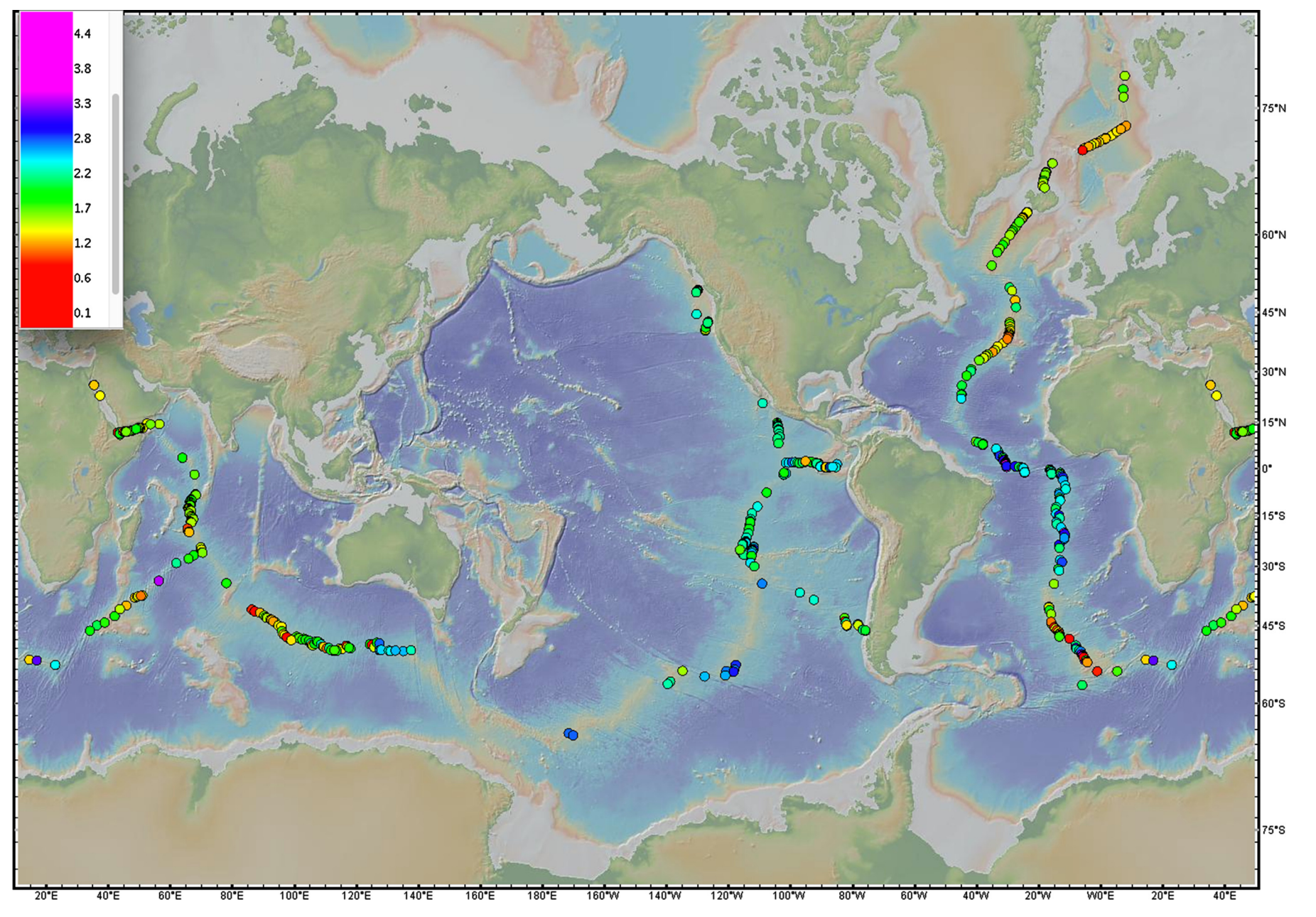


Fig. 8. Global distribution of model depletion ages of sub-ridge mantle. Each circle represents a MORB sample with its mantle depletion age calculated from the measured ⁸⁷Sr/⁸⁶Sr and ¹⁴³Nd/¹⁴⁴Nd isotope ratios. Color legend is mantle depletion age in Ga. The diagram was prepared using GeoMapApp (http://www.geomapapp.org/, Ryan et al., 2009).

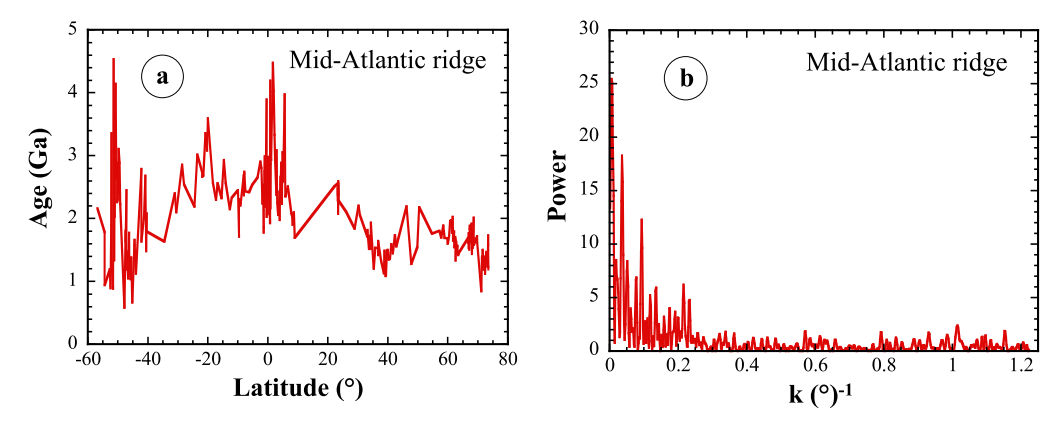


Fig. 9. (a) Sub-ridge Age versus latitude for the mid-Atlantic ridge. (b) Periodogram for the mid-Atlantic ridge.

The sub-ridge mantle of the Pacific ridges mostly has intermediate ages (1.6 to 3.0 Ga). For the Indian Ocean ridges, sub-ridge mantles are mostly between 0.6 to 2.8 Ga, with a mean younger than the mean for the Pacific Ocean ridges. Very old sub-ridge mantles are only found along the mid-Atlantic ridge south of 6°N.

Those age patterns reflect both mantle depletion history and consequences of mantle convection and mixing. For example, the young mantle region beneath the North Atlantic roughly corresponds to the North Atlantic region with high H₂O/Ce ratio (Michael, 1995; Dixon et al., 2002). It is tempting to attribute the young mantle depletion ages of the sub-ridge mantle beneath the Atlantic ridge North of 50°N (including Reykjanes, Kolbeinsey, Mohns and Knipovich ridges) to the effect of the Iceland hotspot. However, the youngest ages are not centered at Iceland, but rather at Mohns ridge. Sub-ridge mantle regions near some hotspots do show local minimum ages, such as Jan Mayen, Azores, Shona/Meteor, and Bouvet, but not near other hotspots, such as Iceland. Ascension, St. Helena, Marion, Cobb, and Easter. Hence, the effect of mantle hotspots on the mantle depletion ages is not straightforward. The juxtaposition of both young and old mantle depletion domains beneath Atlantic Ridge south of 42°S may be a consequence of mantle convection and imperfect mixing. Hence, our results may provide constraints on mantle geodynamic models. In addition, the inferred mantle depletion factors (Supplementary Table S1) characterize the pre-melting MORB mantle and may be used to estimate the mantle source composition of a given MORB (an example can be found in Table 2), which would allow more detailed modeling of the mantle partial melting process.

The mid-Atlantic ridge is a single and almost continuous ridge with no branches, and hence offers an opportunity for a spectral analysis of unevenly spaced data (Press et al., 1992, section 13.8; Agranier et al., 2005). The age versus latitude data and the Lomb periodogram are plotted in Fig. 9. The peak near $k\approx 0$ (with a period of about 180°) in the periodogram (Fig. 9b) indicates a scattered trend of increasing age from north to south. There are three additional major peaks, corresponding to periodicity of 28° (3100 km), 11° (1200 km), and 4.6° (510 km). In addition, there is major magnitude drop of the power at about ~ 0.24 /degree. These features are between type A and type B spectra in Agranier et al. (2005), which they attributed to hotspot influence and continual reduction of mantle heterogeneities by mantle convection.

5. Summary

In summary, we have developed a model to calculate the depletion age and factor of the mantle source from any pair of Sr and Nd isotope ratios for any basalt derived from a depleted mantle. Applying our model to the large MORB database, we find: (i) The MORB mantle source is highly heterogeneous in terms of incom-

patible trace element concentrations. The reference DMM composition of Salters and Stracke (2004) is close to the average MORB mantle composition, whereas that of Workman and Hart (2005) is an extremely depleted endmember of the MORB mantle, much more depleted than the average MORB mantle. (ii) Model mantle depletion ages are mostly between 0.8 to 3.0 Ga. If there was very early massive mantle depletion that corresponded to early rapid continent formation, such depleted mantle is not seen in the sub-ridge mantle sampled by available MORB data. (iii) There are large-scale patterns in depletion ages of sub-ridge mantle regions. For example, beneath Mid-Atlantic Ridge, mantle depletion ages are young (0.8 to 2.1 Ga) north of 30°N, older (1.6 to 4.5 Ga) between 25°N to 35°S), and mixed (0.6-4.4 Ga) south of 35°S. These patterns reveal history of mantle depletion, mantle convection, and possible imperfect mixing between differently depleted mantles as well as between depleted mantle and other mantle endmembers. The results may be of use to geodynamicists in modeling mantle convection and dynamics. In addition, our model allows the estimation of composition of a specific mantle source that generated a MORB, offering an opportunity to investigate the mantle partial melting process that generated the MORB composition.

Acknowledgements

We thank Vincent Salters and Bill McDonough for their insightful and constructive reviews. This research is partially supported by NSF grants EAR-1524473 and EAR-1829822, and NASA grants NNX15AH37G and 80NSSC19K0782.

Appendix A. Supplementary material

Supplementary material related to this article can be found online at https://doi.org/10.1016/j.epsl.2019.115926.

References

Agranier, A., Blichert-Toft, J., Graham, D., Debaille, V., Schiano, P., Albarede, F., 2005. The spectra of isotopic heterogeneities along the Mid-Atlantic Ridge. Earth Planet. Sci. Lett. 238, 96–109.

Belteney, V.E., Skolotney, S.G., Rozhdestvenskaya, I.I., 2014. New chemical and isotopic data for basalts from the axial segment of the Mid-Atlantic Ridge between the Vema and Mercury fracture zones. Dokl. Earth Sci. 459, 1488–1494.

Bouvier, A., Vervoort, J.D., Patchett, P.J., 2008. The Lu-Hf and Sm-Nd isotopic composition of CHUR: constraints from unequilibrated chondrites and implications for the bulk composition of terrestrial planets. Earth Planet. Sci. Lett. 273, 48–57.

Condie, K.C., 2018. A planet in transition: the onset of plate tectonics on Earth between 3 and 2 Ga? Geosci. Front. 9, 51–60.

Connelly, J.N., Bizzarro, M., Krot, A.N., Nordlund, A., Wielandt, D., Ivanova, M.A., 2012. The absolute chronology and thermal processing of solids in the solar protoplanetary disk. Science 338, 651–655.

Cousens, B., Weis, D., Constantin, M., Scott, S., 2017. Radiogenic isotopes in enriched mid-ocean ridge basalts from Explorer Ridge, northeast Pacific Ocean. Geochim. Cosmochim. Acta 213, 63–90.

- Dixon, J.E., Leist, L., Langmuir, C., Schilling, J.G., 2002. Recycled dehydrated lithosphere observed in plume-influenced mid-ocean-ridge basalt. Nature 420, 385–389.
- Gale, A., Dalton, C.A., Langmuir, C.H., Su, Y., Schilling, J.G., 2013. The mean composition of ocean ridge basalts. Geochem. Geophys. Geosyst. 14. https://doi.org/10.1029/2012GC004334.
- Gast, P.W., 1968. Trace element fractionation and the origin of tholeiitic and alkaline magma types. Geochim. Cosmochim. Acta 32, 1057–1086.
- Goldstein, S.L., O'Nions, R.K., Hamilton, P.J., 1984. A Sm-Nd isotopic study of atmospheric dusts and particulates from major river systems. Earth Planet. Sci. Lett. 70, 221–236.
- Gray, C.M., Papanastassiou, D.A., Wasserburg, G.J., 1973. The identification of early condensates from the solar nebula. Icarus 20, 213–239.
- Halliday, A.N., 2004. Mixing, volatile loss and compositional change during impactdriven accretion of the Earth. Nature 427, 505–509.
- Hawkesworth, C.J., Cawood, P.A., Dhuime, B., Kemp, T.I.S., 2017. Earth's continental lithosphere through time. Annu. Rev. Earth Planet. Sci. 45, 169–198.
- Hofmann, A.W., 2014. Sampling mantle heterogeneity through oceanic basalts: isotopes and trace elements. In: Treatise on Geochemistry, 2nd ed., pp. 67–101.
- Jackson, M.G., Dasgupta, R., 2008. Compositions of HIMU, EM1, and EM2 from global trends between radiogenic isotopes and major elements in ocean island basalts. Earth Planet. Sci. Lett. 276, 175–186.
- Jacobsen, S.B., Wasserburg, G.J., 1979. The mean age of mantle and crustal reservoirs. J. Geophys. Res. 84, 7411–7427.
- Jacobsen, S.B., Wasserburg, G.J., 1984. Sm-Nd isotopic evolution of chondrites and achondrites, II. Earth Planet. Sci. Lett. 67, 137–150.
- Kim, J.S., Pak, S.J., Moon, J.W., Lee, S.M., Oh, J., Stuart, F.M., 2017. Mantle heterogeneity in the source region of mid-ocean ridge basalts along the northern Central Indian Ridge (8°S-17°S). Geochem. Geophys. Geosyst. 18, 1419–1434.
- Langmuir, C.H., Bender, J.F., Bence, A.E., Hanson, G.N., Taylor, S.R., 1977. Petrogenesis of basalts from the FAMOUS area: Mid-Atlantic Ridge. Earth Planet. Sci. Lett. 36, 133–156.
- Mallick, S., Dick, H.J.B., Sachi-Kocher, A., Salters, V.J.M., 2014. Isotope and trace element insights into heterogeneity of subridge mantle. Geochem. Geophys. Geosyst. 15, 2438–2453.
- McDonough, W.F., Sun, S.-S., 1995. The composition of the Earth. Chem. Geol. 120, 223–253.
- Michael, P.J., 1995. Regionally distinctive sources of depleted MORB: evidence from trace elements and H₂O. Earth Planet. Sci. Lett. 131. 301–320.
- Moller, A., Mezger, K., Schenk, V., 1998. Crustal age domains and the evolution of the continental crust in the Mozambique belt of Tanzania: combined Sm-Nd, Rb-Sr, and Pb-Pb isotopic evidence. J. Petrol. 39, 749–783.
- Palme, H., O'Neil, H.S.C., 2014. Cosmochemical estimates of mantle composition. In: Treatise on Geochemistry, pp. 1–39.
- Palme, H., O'Neill, H.S.C., 2004. Cosmochemical estimates of mantle composition. In: Holland, H.D., Turrekian, K.K. (Eds.), Treatise on Geochemistry. Elsevier, Amsterdam, pp. 1–38.
- Patchett, J., 1983. Hafnium isotope results from mid-ocean ridges and Kerguelen. Lithos 16, 47–51.
- Pollack, H.N., 1986. Cratonization and thermal evolution of the mantle. Earth Planet. Sci. Lett. 80, 175–182.
- Press, W.H., Flannery, B.P., Teukolsky, S.A., Vetterling, W.T., 1992. Numerical Recipes. Cambridge University Press, Cambridge, England.

- Ryan, W.B.F., Carbotte, S.M., Coplan, J.O., O'Hara, S., Melkonian, A., Arko, R., Weissel, R.A., Ferrini, V., Goodwillie, A., Nitsche, F., Bonczkowski, J., Zemsky, R., 2009. Global multi-resolution topography synthesis. Geochem. Geophys. Geosyst. 10, Q03014. https://doi.org/10.1029/2008GC002332.
- Salters, V.J., Stracke, A., 2004. Composition of the depleted mantle. Geochem. Geophys. Geosyst. 5, Q05004.
- Salters, V.J.M., Mallick, S., Hart, S.R., Langmuir, C.E., Stracke, A., 2011. Domains of depleted mantle: new evidence from hafnium and neodymium isotopes. Geochem. Geophys. Geosyst. 12, Q08001. https://doi.org/10.1029/2011GC003617.
- Shaw, D.M., 1970. Trace element fractionation during anatexis. Geochim. Cosmochim. Acta 34, 237–243.
- Shinjo, R., Meshesha, D., Orihashi, Y., Haraguchi, S., Tamaki, K., 2015. Sr-Nd-Pb-Hf isotopic constraints on the diversity of magma sources beneath the Aden Ridge (central Gulf of Aden) and plume-ridge interaction. J. Mineral. Petrol. Sci. 110, 97–110.
- Shirey, S.B., Walker, R.J., 1998. The Re-Os isotope system in cosmochemistry and high-temperature geochemistry. Annu. Rev. Earth Planet. Sci. 26, 423–500.
- Skolotnev, S.G., 2014. New isotope data for mid-Atlantic Ridge basalts from the Arkhangelsk-Sierra Leone Fracture Zone (central Atlantic). Dokl. Earth Sci. 459, 1429–1435.
- Stracke, A., Salters, V.J.M., Sims, K.W.W., 1999. Assessing the presence of garnet-pyroxenite in the mantle sources of basalts through combined hafnium-neodymium-thrium isotope systematics. Geochem. Geophys. Geosyst. 1, 1006. https://doi.org/10.1029/1999GC000013.
- Stracke, A., Snow, J.E., Hellerbrand, E., von der Handt, A., Bourdon, B., Birdaum, K., Gunther, D., 2011. Abyssal peridotite Hf isotopes identify extreme mantle depletion. Earth Planet. Sci. Lett. 308, 359–368.
- Villa, I.M., De Bievre, P., Holden, N.E., Renne, P.R., 2015. IUPAC-IUGS recommendation on the half-life of 87Rb. Geochim. Cosmochim. Acta 164, 382–385.
- Wilde, S.A., Valley, J.W., Peck, W.H., Graham, C.M., 2001. Evidence from detrital zircons for the existence of continental crust and oceans on the Earth 4.4 Gyr ago. Nature 409, 175–178.
- Workman, R.K., Hart, S.R., 2005. Major and trace element composition of the depleted MORB mantle (DMM). Earth Planet. Sci. Lett. 231, 53–72.
- Workman, R.K., Hart, S.R., Jackson, M., Regelous, M., Farley, K.A., Blusztajin, J., Kurz, M., Staudigel, H., 2004. Recycled metasomatized lithosphere as the origin of the Enriched Mantle II (EM2) end-menmber: evidence from the Samoan volcanic chain. Geochem. Geophys. Geosyst. 5, Q04008.
- Yang, A.Y., Zhao, T.P., Zhou, M.F., Feng, X.G., 2017. Isotopically enriched N-MORB: a new geochemical signature of off-axis plume-ridge interaction a case study at 50°28'E, southwest Indian Ridge. J. Geophys. Res., Solid Earth 122.
- York, D., 1969. Least-squares fitting of a straight line with correlated errors. Earth Planet. Sci. Lett. 5, 320–324.
- Zhang, Y., 2014. Quantification of the elemental incompatibility sequence, and composition of the "superchondritic" mantle. Chem. Geol. 369, 12–21.
- Zhang, W., Zeng, Z., Cui, L., Yin, X., 2018. Geochemical constraints on MORB composition and magma source at East Pacific Rise between 1°S and 2°S. J. Ocean Univ. China (Ocean. Coast. Sea Res.) 17, 297–304.
- Zindler, A., Hart, S., 1986. Chemical geodynamics. Annu. Rev. Earth Planet. Sci. 14, 493–571.